Hindawi
Advances in Civil Engineering
Volume 2022, Article ID 1658021, 20 pages
https://doi.org/10.1155/2022/1658021

Research Article

Study of Instability Mechanism and Roof Caving Mode of Cementing Filling Stope: The Case Study of a Nonferrous Metal Mine in China

Min Zhong,[1,2] **Peng Yang**,[1,3] **and Ying-Peng Hu**[2]

[1]*School of Civil and Resource Engineering, University of Science and Technology Beijing, Beijing 100083, China*
[2]*School of Environment and Resources, Southwest University of Science and Technology, Mianyang, Sichuan 621010, China*
[3]*Beijing Key Laboratory of Information Service Engineering, Beijing Union University, Beijing 100101, China*

Correspondence should be addressed to Ying-Peng Hu; huyan_nice@163.com

Received 28 December 2021; Revised 25 March 2022; Accepted 13 April 2022; Published 9 May 2022

Academic Editor: Gaofeng Song

The downward layered cemented filling method, which is generally used in the mining of high-value metal mines with poor surrounding rock quality, is widely believed to not cause large-scale instability of the roof strata in the mining area. However, a nonferrous metal mine in northern China, which has been using the downward cemented filling method, suddenly suffered a violent collapse accident of the stope roof, and the surface is accompanied by significant subsidence on a large scale. The accident revealed that the roof collapse mechanism still needed further research. In this paper, field investigation and numerical simulation were combined to study the mechanism of roof collapse. Based on the input data including in-situ stress state, geological occurrence pattern, and mining steps, the particle flow code (PFC) was used to simulate the stress and displacement changes of the rock mass under mining disturbance. These results indicate that the failure process of the overlying rock mass can be divided into four stages due to the special geological conditions of the mine: pillar stability stage, pillar chain failure stage, roof filling caving stage, and gneiss plug settlement stage. In the early stage of mining, the pillars between the mined-out drifts could effectively support the overlying rock mass due to the small exposed roof. As more drifts were mined, the vertical pressure on the pillars was added. When the number of mining drifts reached five, one of the pillars was firstly destroyed due to overloading, and then the pressure of the overlying strata was transferred to the surrounding pillars, leading to the subsequent failure of other pillars. When pillars were damaged, arch caving appeared inside the roof filling material. Finally, the vertical shear resistance capacity of the gneiss mass above is insufficient, owing to the steeply dipping joints. Finally, the gneiss above was subject to sudden plug settlement along the vertical joints. It should be noted that the stope mining management of the mine has a significant impact on production safety. In order to ensure the stability of the stope formed by cemented filling method, the dense distribution of simultaneous mining drifts should be avoided and the mine-out areas should be backfilled in time.

1. Introduction

Underground mining would destroy the equilibrium state of the rock mass and eventually lead to surface deformation, which threatens the safety of people and surface structures. The study of this complex process is not only of great practical significance but also of great interest. It is widely believed that the caving method causes the most severe surface subsidence [1–3]. In the process of overlying rock mass caving caused by the goaf, the caving failure will develop upward according to the arch shape, due to the stress arch. Surface damage caused by caving failure is also a progressive process. When the caving failure is transmitted to the surface, a small collapse pit will be formed at first, then the cracks will loosen under the action of tensile stress, and finally, the collapse pit will gradually expand due to the lateral collapse of the surrounding rock mass [4–7].

Engineering geological conditions (joints, faults, and surface morphology, etc.) also affect the development form, process, and scope of surface collapse. Joints will affect the

development direction of caving failure and the range of surface failure will change accordingly. Faults near mining areas also inhibit the spread of surface damage. The various and complex topography can also lead to multiple failure modes, such as landslides caused by underground mining under mountains [8–10].

In contrast, the filling method can effectively suppress surface deformation. Backfilling goaf with cement dry material can effectively restrain further deformation of the surrounding rock. Meanwhile, cementing materials applied to backfill goaf such as cement slurry can significantly reduce the displacement of rock strata [11, 12]. By constantly backfilling the goaf, the existing goaf is small and scattered. This improves the stress state of the surrounding rock, and the narrow mined-out area also inhibits the failure expansion of the surrounding rock mass, so the filling method generally does not cause severe surface failure. Even when the surface deforms, it is slight and slow subsidence.

Many studies have been carried out by researchers to study the deformation mechanism of surface subsidence through theoretical analysis, physical modelling, field observation, and numerical simulation. In terms of theoretical research, Ding et al. analyzed the mechanism of surface deformation caused by underground mining in the Hemushan Iron Mine through the elastic mechanics method, predicted the damage range of the surrounding rock of the cylindrical caved space, and revealed the impact of the gravel on the stability of the caved space [13]. However, there have been only a few theoretical studies due to the complexity of the problem. Moreover, most theoretical models are based on many simplifications. Therefore, it is difficult to explain the rock mass failure mechanism caused by mining under complex conditions through theoretical formulas.

As for physical modelling, Ghabraie used physical modelling to investigate the surface subsidence mechanism and substrata movement characteristics [14]. Ren constructed a physical model to simulate the deformation and failure of ground surface and rock mass around the mined-out area [15]. Due to the use of similar materials that can reproduce the similar characteristics of the in-situ rock mass characteristics, the simulation results are intuitive and related to the actual situation. However, for the operability of the experiment, some artificial uncertainties are often introduced, so the physical model cannot fully reproduce the surface subsidence and rock failure process in the field.

Field monitoring is the most direct method of surface deformation research, and the monitoring data can truly reflect the surface displacement law. Surface monitoring methods including theodolite, total station, and global positioning system (GPS). For example, GPS is applied to monitor the surface deformation of many metal mines, such as Kiirunavaara mine, Jinchuan Nickel mine, and Chengchao Iron Mine, and the detailed monitoring data obtained are used to analyze the surface deformation characteristics and formation movement mechanism caused by underground mining [16–18]. The deformation of deep strata can be monitored by microseismic and extensometer [19, 20]. However, these field monitoring methods are limited to recording ground deformation, and mechanical mechanism analysis is lacking. Therefore, stress redistribution and fracture initiation and propagation caused by underground mining cannot be revealed only by the monitoring data.

In recent years, the development of computer technology has made numerical simulation a low-cost and efficient research method. Much simulation software based on different principles has been used to study surface subsidence and rock movement caused by mining. According to the calculation principle, these pieces of simulation software can be divided into three categories: (1) continuous medium method, namely, FLAC3D, RFPA2D, ABAQUS, etc. [7, 21, 22]; (2) discontinuous medium method, namely, UDEC, 3DEC, DDA, PFC2D, etc. [23–30]; and (3) Mixed methods, namely, ELFEN [8, 31, 32].

The continuum method considers the model as a continuous and inseparable object. The continuum method can reveal the stress distribution characteristics of the surrounding rock caused by underground mining and obtain the final surface damage range [33]. Because the elements in the continuum method cannot be separated, it is naturally difficult to simulate the collapse separation process of the surrounding rock. For the discontinuous medium method, the numerical model consists of many discontinuous elements, which are connected by bond elements. Once some limit conditions are met, the bond element is broken so that the discrete element is separated. In this way, the large deformation of the rock mass can be simulated and the collapse process of the rock mass can be reproduced [24, 26–30].

One of the key factors for reliable numerical simulation is the correct selection of parameters. The mechanical parameters of small intact rock can be measured through laboratory experiments. However, for the engineering scale, the mechanical response characteristics of large rock mass with random geological features such as joints are different from those of small intact rock. The Hoek–Brown criterion is widely regarded as an effective method to obtain the calculated parameters of rock mass in engineering scale. Due to the subjective judgment involved in this evaluation method, the back analysis of the parameters should be carried out based on the existing failure phenomenon [33].

The filling method is effective in inhibiting the deformation of the surrounding rock and maintaining the stability of the stope and surface. However, the surface collapse accident at a nonferrous metal mine in north China deserves more attention.

Due to the poor quality of the rock mass, the mine adopts the downward layered cemented filling method. In the long-term mining process, the surface can maintain a stable state. However, in March 2016, the roof strata of the goaf located 120 m underground suddenly collapsed, and then the surface collapsed violently. The surface area of the collapse pit exceeds 10000 square meters. Severe surface deformation poses a great threat to the safety of surface personnel and structures, and seriously interferes with normal mining. Due to the filling mining method, the mine did not form a large-scale goaf, but several narrow mined-out areas located at the depth of 120 m underground caused sudden caving of the

overlying strata and rapid surface collapse. This failure mechanism and rock movement law are worthy of further study in order to provide the reference for the safety of mining in the next step.

In this paper, we investigate the field damage of the mine, then establish a two-dimensional numerical model using PFC2D. The calculated parameters are obtained by trial-and-error tests referring to field damage. Finally, the whole process from pillar destruction to surface collapse is reproduced. Through field investigation and numerical simulation, the mechanism of instantaneous large-scale surface collapse in a nonferrous mine is studied.

2. Engineering Background

2.1. Ore Body Layout and Mining Situation. The nonferrous metal mine is a nickel mine located in north China and has multiple ore bodies. The 1# ore body is the main industrial ore body, and the plane shape of the ore body is gourd-shaped (Figure 1). The ore body strikes NW30° and dips 50°–80° toward SW, which is mainly located between exploration lines 4 and 12 and is 400 m long.

As shown in Figure 2, the overlying rock layer of the ore body consists of two lithological groups, the surface layer is Quaternary sediments with a thickness of 50 m, and the lower part is gneiss with a thickness of 50 m. Tectonic joint groups exist in gneiss, which is smooth and has weak fillings. There is a fault in this area, which strikes NW and dips 80°–85° toward SW.

The mining area was completed and put into operation in 2010, with a designed annual output of 165 *t*. Due to the poor rock mass quality and high-value ore, downward cemented filling method was adopted to maintain stope stability and reduce loss and dilution, which is shown in Figure 3. There are two sublevels at 1642 m and 1546 m level. As of March 2016, the working face in the upper mining area has reached 1614 m level, forming a 30 m thick cemented filling body. And the working face in the lower mining area has reached 1504 m level, forming a 42.5 m thick cemented filling body. At this time, the stop at the 1613 m level was damaged, resulting in surface collapse. Figure 4 shows the mining status at this time.

2.2. Rock Mass Properties and In Situ Stress. In order to obtain the mechanical properties of the surrounding rock mass and ore body, some relatively complete rock blocks are extracted from the mine and made into standard samples with the diameter of 50 mm and the height of 100 mm. Then, the mechanical properties of the intact rock are obtained by an unconfined uniaxial compression test in the laboratory. The geological strength index (GSI) of rock mass is calculated according to rock quality designation (RQD) values [34]. Finally, the mechanical parameters of rock mass are obtained through the generalized Hoek–Brown criterion [35], as shown in Table 1.

Many in-situ stress measurements have been carried out in the long-term mining process of the mine. The measured value of in-situ stress in the drift near the 5# exploration line at 1610 m level is selected to construct the in-situ stress state of the study area.

The magnitudes and directions of in-situ stress are obtained from the measurement results. The maximum principal stress is 4.2 MPa, of which the dip is 10° and the dip direction is 325°. The middle principal stress is 3.2 MPa, of which the dip is 80° and the dip direction is 145°. And, the minimum principal stress is 0.8 MPa, of which the dip is 3° and the dip direction is 48°.

3. Investigation of Surface and Underground Stope

After long-term mining with the filling method, the nonferrous metal mine has formed the stratum status as shown in Figure 4. The surface remained stable after years of mining. In March 2016, when the 1613 m sublevel was mined, the stope pillars were suddenly destroyed, causing the roof to collapse. At this time, most of the mined-out areas in the mine had been filled, only a few of the mined-out drifts at the level of 1613 m had not been filled yet. However, the destruction of the overlying strata was still developing rapidly and then the surface collapsed violently. In order to reveal the mechanism of rock failure, detailed field investigations were carried out from the underground stope at 1613 m level to the surface.

The investigation starts from the 1613 m level where the damage first occurred. According to the mining plan, there would be several unfilled drifts at this level before filling together. The height of a single drift is generally only 3–5 m and the width is only 4–6 m. The failure first occurred in these narrow drifts. According to the survey, the damaged area is mainly concentrated between 5# and 7# exploration lines.

As shown in Figure 5, the roof of the drifts between the 5# and 7# exploration lines collapsed, and the collapsed broken rock filled the drifts. Due to the expansion characteristics, the gravel falling from the roof quickly filled the narrow space, so as to restrain the deformation of the surrounding rock.

Therefore, the damage range of the overlying rock mass caused by the deep underground narrow and scattered goaf is limited, and the damage of roof rock mass is difficult to be transmitted to the surface. However, in this case, the overburden of the stope was greatly deformed and the surface collapsed.

In order to study the failure characteristics of the overlying rock mass, field investigations were also carried out at the 1630 m and 1650 m levels. As shown in Figure 6, the drifts at the 1630 m level near the 7# exploration line had an overall staggered settlement of 3 m.

As shown in Figure 7, the drifts between the 5# and 7# exploration line at the 1650 m level had overall subsidence.

The roof of the drift near the 5# exploration line had 0.4 m subsidence, the damage extended about 70 m along the drift, and the bottom of the drift had a subsidence of 2 m (Figure 7(a)). The damage near the 7# exploration line was 60 m along the drift. The roof had obvious fracture damage and staggered subsidence of 0.3 m. The bottom plate had

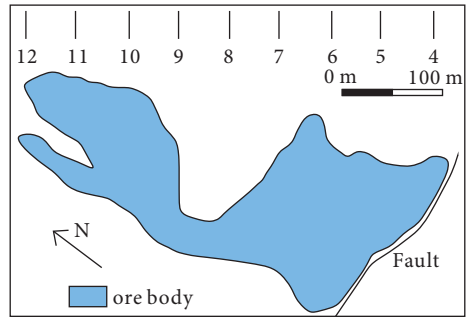

Figure 1: The plane projection map of the 1 # ore body at the 1650 m level.

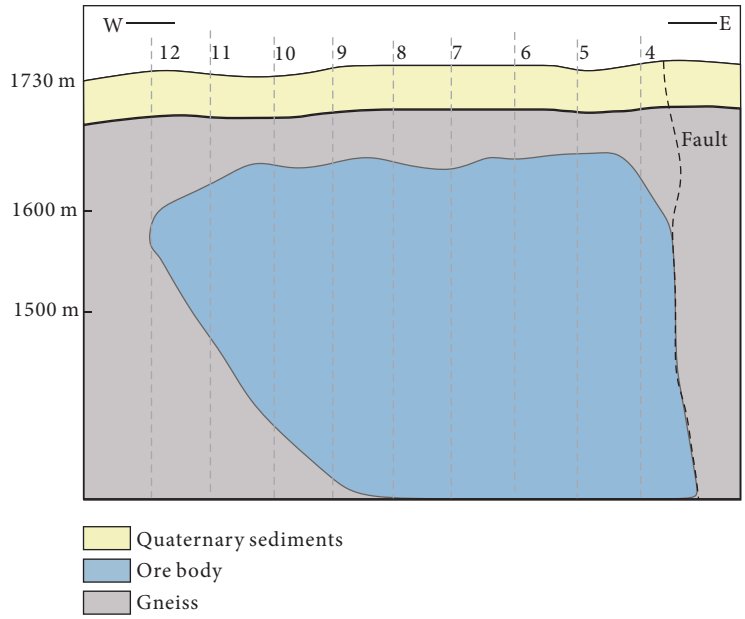

Figure 2: The longitudinal projection map of the 1 # ore body.

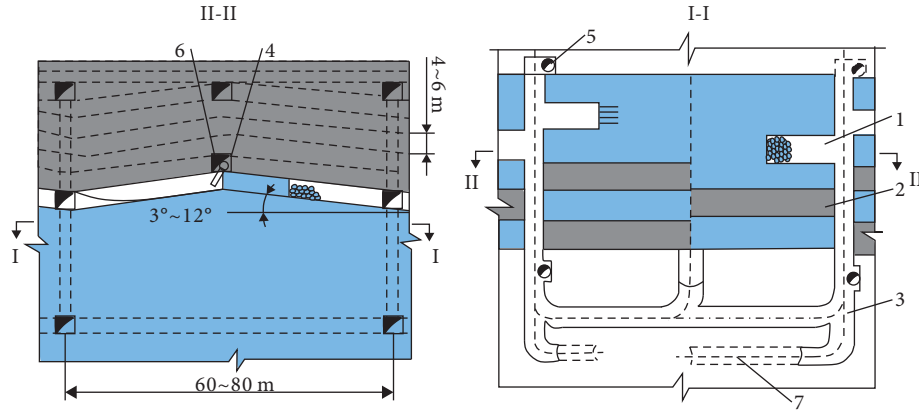

Figure 3: Schematic diagram of the stope of downward cemented filling method. (1-mining drift; 2-filling drift; 3-sublevel haulage road; 4-sublevel filling road; 5-orepass; 6-filling material transportation pipeline; 7-ramp; ore (blue); cemented backfill body (grey)).

greater subsidence, with a settlement of about 1 m (Figure 7(b)). The north side wall of the drift near the 6# exploration line was broken along the drift, with dislocation at the fracture and floor uplift of about 1 m (Figure 7(c)).

Compared with the failure between 5# ~ 7# exploration lines, the rock mass near the 9 # exploration line had no obvious damage, and the roadway could still maintain stability (Figure 7(d)). It can be seen that the rock mass

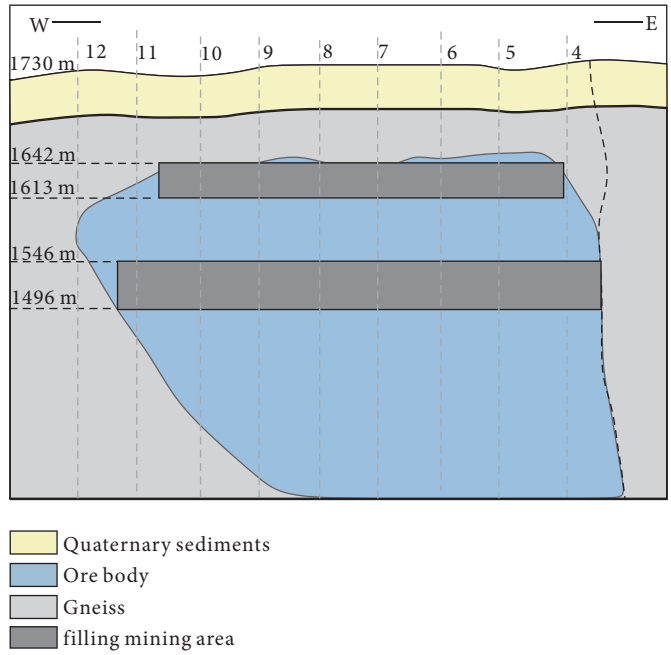

Figure 4: The vertical projection map of mining status.

Table 1: Mechanical parameters of the rock mass.

Rock type	Bulk density (kg/m³)	Compressive strength (MPa)	Tensile strength (MPa)	Elastic modulus (GPa)	Internal friction angle (°)
Gneiss	2700	17.2	1.7	37.2	27
Quaternary	2000	1.7	0.31	8.2	21
Ore body	2800	14.3	1.8	28.1	28
Filling body	2200	6.5	0.8	9.2	23

failure caused by stope instability has an obvious influence range, and the expansion of failure in rock mass was mainly in the vertical direction.

Although the overburden is 80 m thick and the rock mass at this level moves only 1-2 m downward, the movement of the rock stratum is still rapidly transmitted to the surface and causes surface collapse. The collapse pit is still distributed between 5# and 7# exploration line, with an area of more than 10 thousand square meters (Figure 8).

4. Analysis on the Collapse Mode of the Stope Roof

According to a large number of cases, the instability of underground stope may lead to two failure modes of overburden, progressive arch caving failure and sudden plug subsidence [7, 36].

As shown in Figure 9, the arch failure of the rock mass is more common. The roof rock stratum is affected by tension, and the failure surface expands upward in an arch shape. This failure development is gradual, and the collapsed gravel mostly presents a loose state.

Due to the expansion characteristics of loose gravel, if the goaf is small, it will be quickly filled with expanded gravel. Without compensation space, further deformation and failure of surrounding rock are restrained.

Therefore, for the deeply buried goaf, only a large enough goaf can provide enough space to transfer the damage of the roof to the surface. Even if the damage develops to the surface, the surface damage process is gradual. First, cracks appear on the surface, then small collapse pits appear, and finally, the rock mass on the pit wall falls to expand the collapse pit.

Another common failure is plug settlement. After the goaf is formed, the overburden loses its lower support, and the steep weak surface reduces the shear resistance of the roof rock mass. After the through shear surface is formed, the overburden settles rapidly. This kind of damage is rapid, and the roof of the goaf tends to sink as a whole rather than break and collapse (Figure 10).

According to the damage investigation in the previous section, the roof failure mechanism of the nonferrous metal mine is relatively complex. A large number of loose gravels are observed at the 1613 m level, which shows that the roof of the goaf has collapsed. While at the 1630 m

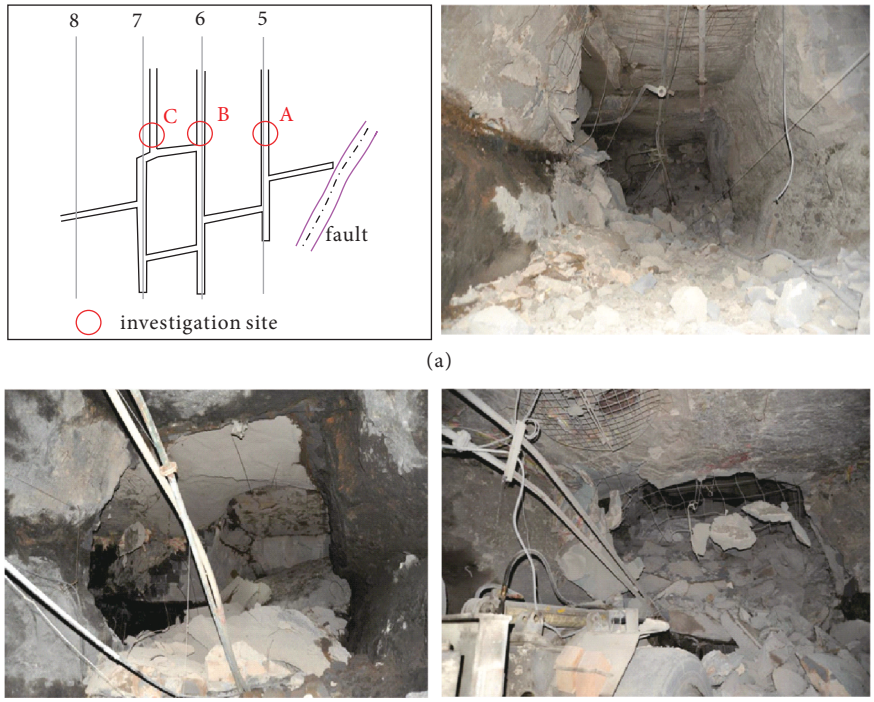

Figure 5: The location of the investigation and the filed destructions at the 1613 m level.

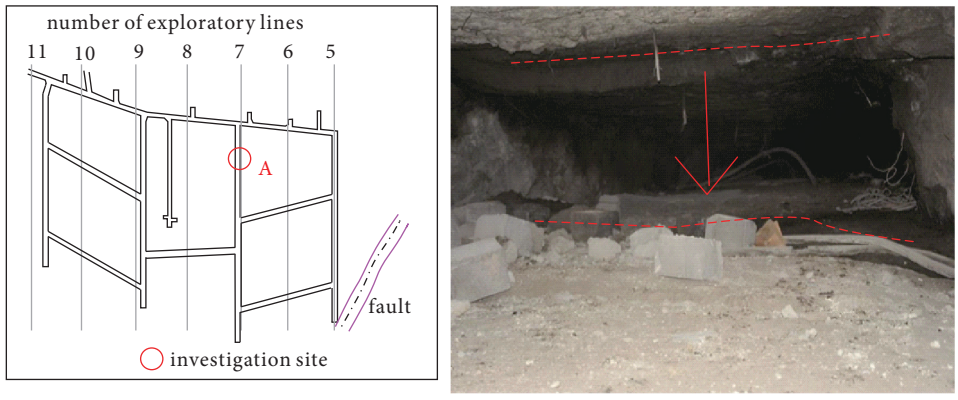

Figure 6: The location of the investigation and the filed destructions at the 1630 m level.

level, about 20 m above the roof, the drift has only sunk as a whole, which shows that the lower caving failure has not developed to this level.

Although, due to inaccessibility, it is impossible to directly observe the height of the caving failure of the roof, the development height of the failure can be estimated by theoretical calculation. Assuming that the height of the initial goaf is H_1, the height of the roof failure is H_2.

The crushing expansion coefficient is η; then, the height of the crushed rock pile is $\eta \cdot H_2$; the height of the gap between the top of the crushed rock pile and the goaf is Δ; and the spatial relationship is shown in Figure 11.

Then, the gap can be calculated according to the following formula:

$$\Delta = H_2 + H_1 - \eta H_2. \quad (1)$$

When $H_1 = H_2(\eta - 1)$, $\Delta = 0$.

At this time, the falling loose bodies will fill the mined-out area, and there is not enough space to

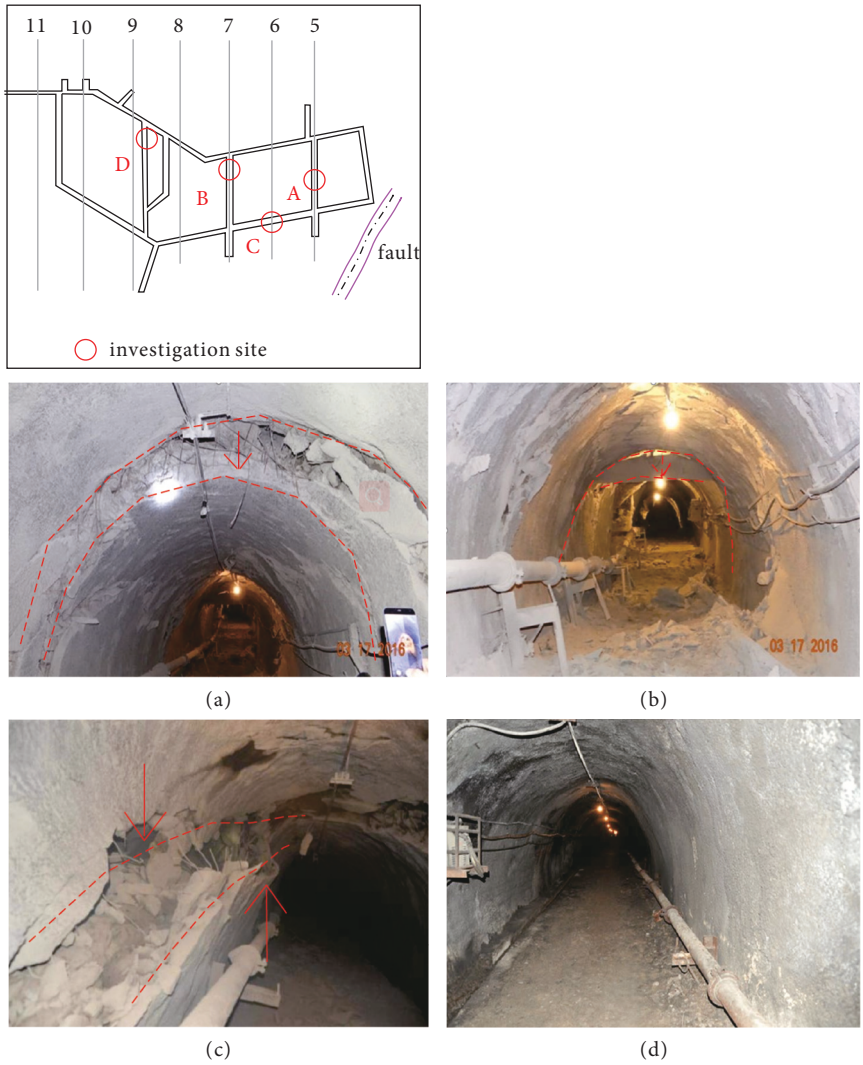

Figure 7: The location of the investigation and the filed destructions at the 1650 m level.

accommodate the broken roof rock mass. When the falling debris is full of the mined-out area, the falling height of the roof can be calculated as follows:

$$H_2 = \frac{H_1}{(\eta - 1)}. \tag{2}$$

The looseness coefficient is the ratio of the volume of gravel to the volume of intact rock mass. So, it has no units. The height of the mine-out area is the layered height of 5 m. Substituting the above data into equation (2), it can be got that,

$$H_2 = \frac{H_1}{\eta - 1} = \frac{5}{1.5 - 1} = 10\,\text{m}. \tag{3}$$

It can be seen that the caving failure of the roof stops when it develops to the level of 1628 m. At this time, the goaf is filled with gravels. Gneiss is located above the 1642 m level. Due to the steep dominant joint surface of the gneiss, the shear resistance of overlying strata can only be provided by the shear strength and friction between joints. However, according to the geological data and field investigation, there are weak interlayers between the joints in gneiss, and the shear resistance is poor. Although the arch caving failure did not develop into gneiss, the failure of the lower filling material led to the decline of support capacity. When the supporting force of the lower part and the shear resistance of the lateral joint cannot bear the gravity of the overlying strata, the gneiss will sink along the joint in a piston manner. The overall staggered subsidence of the roadway shown in Figures 6 and 7 is favorable to prove that the gneiss has overall plug subsidence.

Therefore, the stope instability of the nonferrous metal mine leads to a composite failure mode of the overlying strata. In this mode, the lower filling body has arched caving, and the upper gneiss has instantaneous plug settlement as shown in Figure 12.

5. Study on the Mechanism of Stope Instability

Because this accident involves rock mass collapse and large surface deformation, it is more necessary to reveal the whole process from the initial fracture to the large-scale instability of the overlying strata.

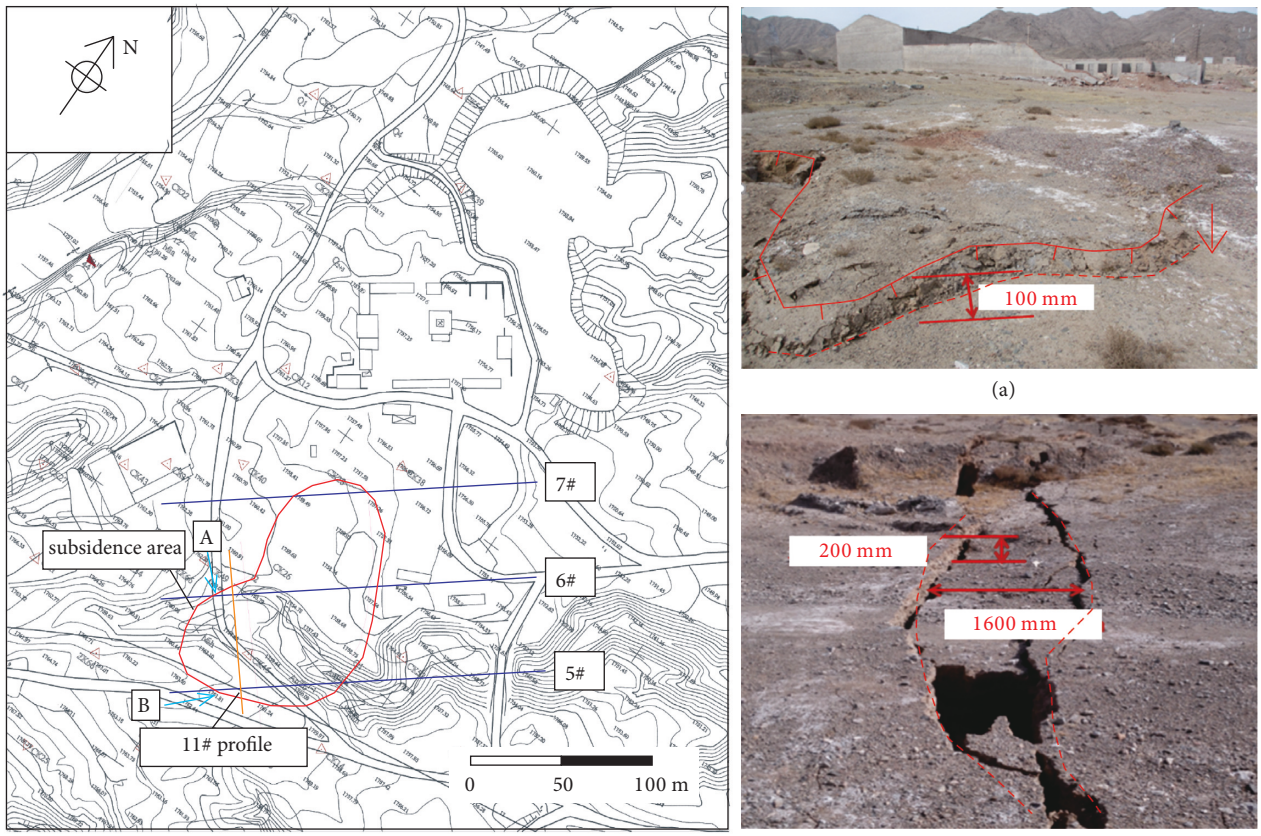

Figure 8: The location of the investigation and the damage at the site on the surface.

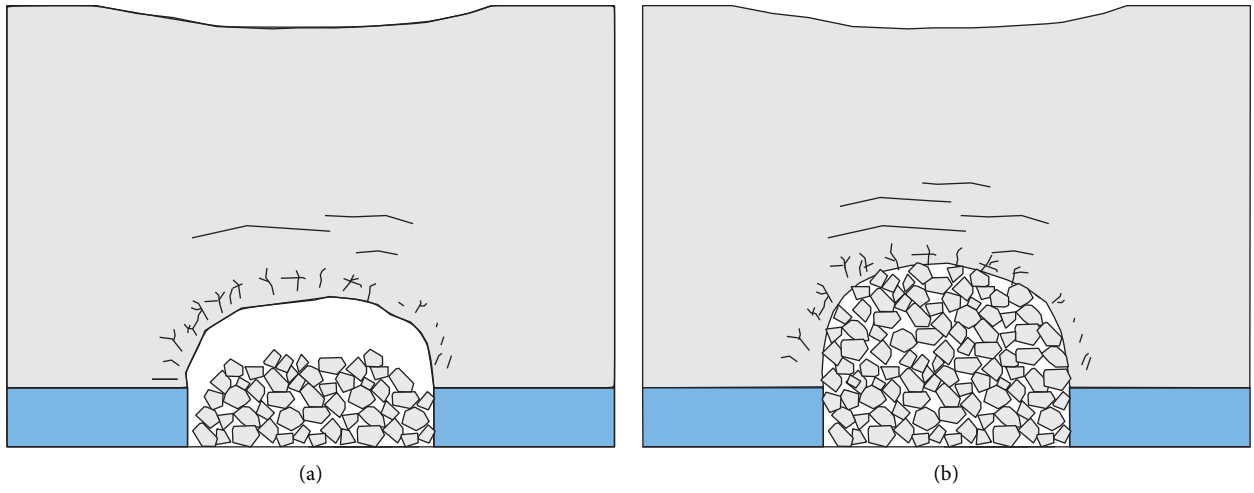

Figure 9: The process of arched caving in the roof strata. (a) Initial caving of the roof strata. (b) Natural termination of rock strata fall.

Compared with the continuous medium method, the discrete element method is more suitable for the case study. Based on the discrete element method (DEM), the particle flow code (PFC) uses an assembly of cemented particles to simulate the intact material. The PFC can simulate the whole process of the rock mass from crack initiation to disintegration depending on its particle flow characteristics. The contact between particles makes the development process of material failure more realistic. Therefore, the PFC has been successfully applied to the research in the field of mining engineering [37–39].

Diego used the PFC to study synthetic rock mass (SRM) modelling techniques, successfully simulating the mechanical behavior of jointed rock masses, and obtained predictions of rock mass scale effects, anisotropy, and brittleness [40]. Svartsjaern studied the gradual collapse process of the

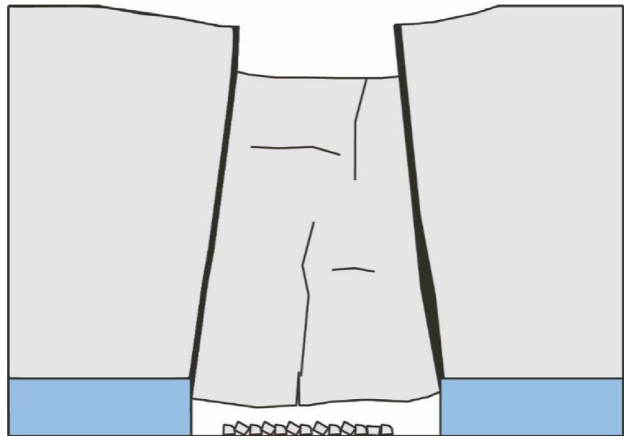

Figure 10: The plug subsidence of the overlying strata.

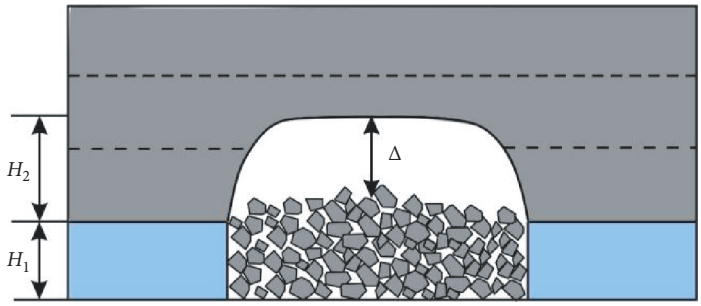

Figure 11: Schematic diagram of roof caving.

ground surface induced by sublevel caving at the Kiirunavaara Mine with the PFC, and the simulation results were consistent with the actual situation [28]. Li studied the mechanical mechanism of surface subsidence and filling material movement caused by underground mining in Hongling lead-zinc mine through the PFC [41]. It is revealed that the collapsed waste rock in the mined-out area can provide support force for the surrounding rock and restrict the further collapse of the hanging wall.

5.1. Microscopic Parameter Calibration and Numerical Model Setup. In this study, the two-dimensional particle flow code (PFC2D) was used to investigate the mechanism of strata movement and surface subsidence induced by underground mining. The basic contact model between particles is generally the contact bond model (CBM) or the parallel bond model (PBM). The contact bond can only transmit the force, while the parallel bond can transmit both force and moment between particles. The PBM is a more realistic bond model for modelling the rock-like material and has been successfully used in previous studies, which was therefore adopted in this study [37–39, 41].

Parallel bonds break when the maximum tensile stress of parallel bonds between particles exceeds their tensile strength or the maximum shear stress of parallel bonds exceeds their shear strength under external forces. This results in the formation of micro-tension or shear cracks. When many adjacent micro-cracks occur, they connect with each other and form large cracks, which lead to the failure of the complete material. Finally, the bond behavior is replaced by the loose behavior.

In addition to the above two contact models, the PFC also contains a smooth joint model (SJM) which can effectively simulate the mechanical response of joints in the rock mass. The smooth-joint model simulates the behavior of a planar interface with dilation regardless of the local particle contact orientations along the interface. In this model, particles are allowed to slide past one another without over-riding one another. It is a major breakthrough to represent discontinuities as planar surfaces associated to a realistic behavior for structural defects [42–44].

Therefore, the PFC model using the parallel bond and smooth joint model is suitable for simulating the whole process of cracking and breaking of rock mass.

The PFC uses an assembly of bonded particles to simulate the mechanical response of rock mass, of which the model parameters are to describe the mechanical properties between particles, such as the normal stiffness and shear stiffness of the contacts. These microscopic parameters are not directly and necessarily related to the macroscopic mechanical parameters of the rock mass simulated by the particle assembly. Therefore, a series of numerical simulation experiments (uniaxial compression, tensile strength test, biaxial compression test, etc.) are required to conduct trial-and-error tests to obtain the mechanical parameters of the microscopic particles that match the actual rock mass

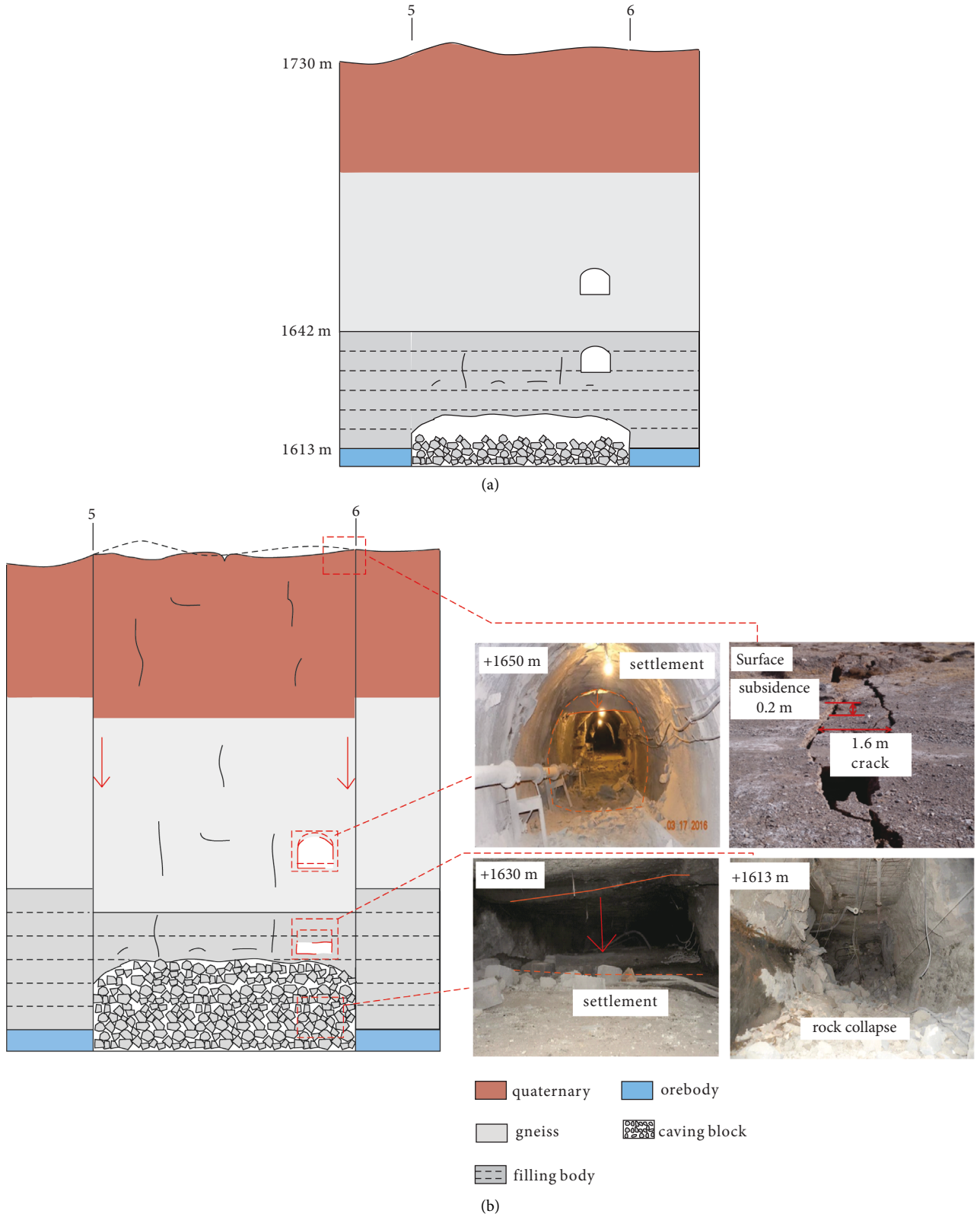

Figure 12: The failure process of overburden rock formation caused by underground mining. (a) Step 1: Arched caving of the roof filling body. (b) Step 2: Plug-subsidence of the upper gneiss.

Table 2: Microscopic parameters of the rock.

Parameters	Value			
	Gneiss	Ore body	Filling body	Quaternary soil
Density (kg/m^3)	2700	2800	2200	2000
Contact bond modulus (GPa)	17.94	14.35	4.36	4.36
Contact bond stiffness ratio	1.57	1.57	1.57	1.57
Friction coefficient	0.25	0.25	0.25	0.25
Parallel bond tensile strength (MPa)	5.79	4.63	2.07	0.56
Parallel bond cohesion (MPa)	4.83	3.86	1.73	0.47
Parallel bond friction angle (°)	40	42	39	38
Parallel bond modulus (GPa)	17.94	14.35	4.36	4.36
Parallel bond stiffness ratio	1.57	1.57	1.57	1.57

parameters [41]. According to the rock mass parameters shown in Table 1, the corresponding microscopic parameters are shown in Table 2.

The mechanical parameters of joints are often difficult to obtain, which usually need to be judged by experience according to the field conditions. Because additional parameter matching process is needed in the PFC model, it is too complex to obtain the micro parameters corresponding to the actual joints in PFC simulation. It is widely recognized that the strength of joints is much lower than that of rocks. Therefore, the reduction of the strength parameters of the smooth joint model can also effectively reflect the mechanical response characteristics of joints in the model, and the final effect of this simulation also proves this feasibility. The joint parameters shown in Table 3 are used in this paper.

The 11 # profile in Figure 8 is selected as the research object. Due to the complex geological conditions, the profile is moderately simplified on the premise of retaining the main engineering geological elements, as shown in Figure 13. According to this profile, a two-dimensional numerical model including 122087 particles is established in the PFC to simulate the rock strata movement caused by underground mining (Figure 14).

In this mine, filling mining has been carried out simultaneously at both levels, forming the engineering geological status as shown in Figure 4. The failure occurred in the upper mining area, so the model only included the strata above the 1613 m level. Four rock strata are successively distributed in the model from top to bottom, which are 50 m thick Quaternary strata, 50 m thick gneiss, 30 m thick cemented filling body, and 15 m thick ore body, respectively, as shown in Figure 14. There are two groups of dominant joints in the gneiss, the projection of which in this section is horizontal (dip 3°) and vertical (dip 88°), respectively. Geological data show that the joints in gneiss have good continuity, so the joints in the model are assumed to be consecutive joints. To simplify the model, the joint spacing is enlarged by integer multiples. Although this change will reduce the authenticity of simulation results in some aspects, it can still explain the failure mechanism of the roof in essence. At the same time, due to the filling process, there is a hexagonal contact surface of the filling body in the filling body, which is also considered as a kind of joint. Finally, considering the simulation accuracy and simulation efficiency, the particle radius is 0.25 m–0.38 m.

5.2. Model Boundary Conditions. In-situ stress should be applied to the model prior to numerical simulation of underground mining. The vertical stress is set as gravity, while the direction of horizontal stress is not in the same plane as the strike direction of the 11 # profile. Therefore, before being applied to the model, the horizontal stress should be first converted to the inclination direction of the profile, and the horizontal stress of the profile is 4.2 MPa.

The initial stress is applied to the PFC model through the following procedure. In the first stage, the top of the PFC model was unconstrained to maintain the natural state, and the wall boundary constraints were adopted at the bottom and both sides. The displacements of both sides and the bottom boundary were fixed; then gravity was applied to each particle of the model. Finally, the model was run to balance. In the second stage, the horizontal displacement of the left and right walls was released to adjust the horizontal pressure on the model. The FISH language built in the PFC was used to compile the servo program, which could adjust the position of the walls to make the actual horizontal in-situ stress of 4.2 MPa on the model according to the monitored pressure on the wall. In the third stage, sufficient time steps were run to make the model reach the equilibrium state.

5.3. Simulation Schemes and Measurement Schemes. In this study, the PFC2D is used to simulate the surface collapse accident caused by underground mining in a nonferrous metal mine, and the process and mechanism of the movement of overburden strata ultimately caused by the instability of several narrow mined-out areas are studied.

The downward layered cemented filling method has always been adopted in this mine. First, it was mined along the drifts and cemented filling was carried out after the mining was completed. After the filling body was cured, the adjacent drifts were exploited again. In order to improve the mining efficiency, cemented filling was usually only carried out once after 5 drifts had been exploited. The damage happened just after the five drifts were mined and before the filling was completed. Therefore, in this simulation, 6 drifts were planned to be exploited sequentially from the middle to both sides. As shown in Figure 15, the drifts were numbered from 1 # to 6# according to the mining sequence.

In order to record the stress evolution of roof and pillar during excavation, a set of stress measuring circles was set up

Table 3: Microscopic parameters of the joints.

Joint type	Normal stiffness (GPa)	Shear stiffness (GPa)	Friction coefficient	Cohesion (Pa)	Tensile strength (Pa)
Dominant joint of the gneiss	15.0	10.0	0.1	$2.50E+04$	$1.00E+04$
Boundary surface of the filling body approach	15.0	10.0	0.1	$6.00E+03$	$4.00E+03$

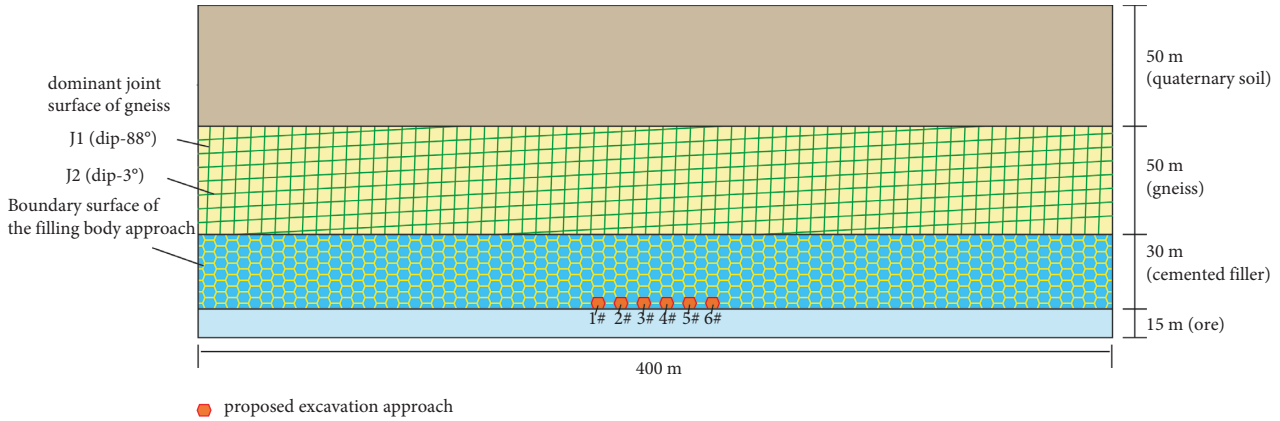

Figure 13: Schematic diagram of the simplified 11# profile.

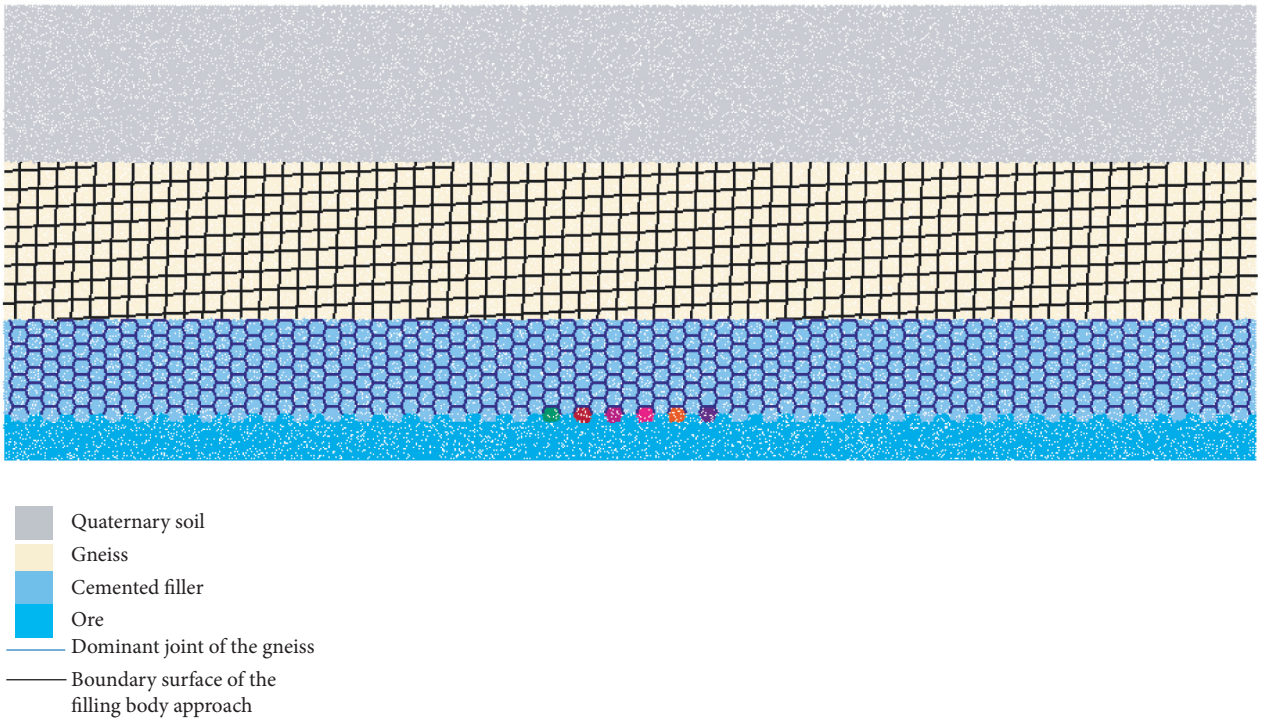

Figure 14: The PFC numerical model of the simplified 11# profile.

in the model as shown in Figure 15. The radius of the stress measuring circle in pillars is 3 m (from 1 to 5), and that in the roof is 4 m (from 6 to 8).

5.4. Numerical Results and Analysis. In this section, the mechanical mechanism of the strata movement and surface collapse caused by underground mining is studied. Figure 16 shows the failure process and corresponding stress evolution of rock mass during excavation simulation. The left figure shows the failure process of rock mass during simulation, in which the red mark is the location of particle bond fracture to characterize the failure cracks of the rock mass. The right figure shows the distribution of contact force, which reflects the transfer path of force inside the model. Blue lines

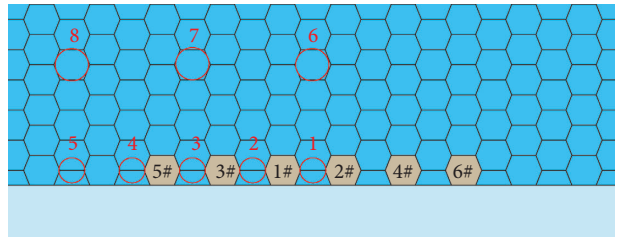

Figure 15: Layout of stress measurement circles and drifts mining sequence (Circles 1–8 are stress measurement circles; the mining sequence of the drifts is from 1 # to 6 #).

indicate compressive force, red indicates tensile force, and line thickness indicates the magnitude of force.

As shown in Figures 16(a) and 16(b), after excavation of the 1 # drift, the surrounding rock can be maintained stable with only a few cracks in the roof. Excavation results in a stress state change of the surrounding rock. Tensile stress occurs in the roof, where compressive stress decreases. And, the concentration of compressive stress occurs on both sides of the drift.

As shown in Figures 16(c) and 16(d), the roofs remain stable and the pressure of the intermediate pillar is significantly concentrated after excavation of the two approaches.

After excavation of three drifts, the stope remains stable despite the increase of cracks in the roof of the 1# drift. Figure 16(f) shows that a smaller stress arch occurs in the roof at this time, which is a sign of further roof failure, with pressure apparently concentrated towards both pillars. When four drifts are excavated, the pressure of the pillars increases further, but the stability can be maintained.

When five adjacent drifts are mined, the vertical stress on the pillars exceeds their strength limit and cracks are found throughout the pillars. The force chain inside the four pillars disappears, indicating that the pillars have lost their bearing capacity at this time. A lot of tension cracks and stress arching appear in the roof filling body. The vertical pressure can only be transmitted to both sides along the stress arch, and the compressive stress concentration occurs in the surrounding rock outside of the 5# and 4 # drifts. Horizontal joints make gneiss present horizontal layered structure. Under the compression of horizontal in-situ stress exceeding vertical in-situ stress, the layered structure just maintains stability, but this stability is very fragile.

When the number of drifts mined reaches 6, the ore pillar between drift of 4 # and 6# is rapidly destroyed, which further expands the span of the collapsed goaf. Meanwhile, the stress arch in the backfill body is destroyed, the backfill body is broken as a whole and cannot bear the vertical pressure. Cracks develop upward in the overlying gneiss and are widely distributed in the model, developing upward only along vertical joints. As shown in Figure 16(l), the original arch stress in the filling body disappears, and the newly formed random stress chain is the contact force formed by the collapse of the scattered body.

The original horizontal layered force chain in gneiss is destroyed. There are obvious vertical force chains on the left and right sides of the overlying gneiss, while the middle part still maintains the original stress state. It can be seen that vertical shear failure occurs at both sides of the rock mass, while the middle of the gneiss remains intact, that is, plug subsidence occurs. This indicates that the gneiss has undergone plug settlement.

When the number of drifts mined reaches six, as shown in Figures 16(k) and 16(l), the pillar between 4 # route and 6# route is destroyed rapidly, which further expands the span of the goaf. Then, the roof filling body is broken, and the stress arch is completely destroyed, which loses its support capacity.

The cracks only develop upward along the vertical joints in the gneiss above, where they are not widely distributed as in the filling body. As shown in Figure 16(l), after the stress arch in the filling body disappears, the newly formed random force chain shows the contact force generated by the collapse gravels accumulation.

The original horizontal layered force chain in gneiss is destroyed. There are obvious vertical force chains on the left and right sides of the overlying gneiss, while the middle part still maintains the original stress. It can be seen that vertical shear failure occurs at both sides of the gneiss, while that of the middle remains intact. This indicates that the gneiss has undergone plug settlement.

As shown in Figure 17, the evolution of the vertical displacement cloud diagram of the model during mining also clearly reflects the failure process of the rock mass. When four drifts are exploited, the roof strata can still maintain stability. When five drifts are mined, the roof filling body has arched caving; after six drifts are mined, the arched caving damage of the backfill body continues to develop upward, and when it develops to the overlying gneiss, it causes plug subsidence of the gneiss along the vertical joints.

In order to monitor the stress evolution process of the surrounding rock and pillar of the stope roof, as shown in Figure 15, several stress measurement circles are arranged in the model. Figure 18 shows the evolution of vertical stress in the pillar and roof strata, respectively, during the mining process. When the first drift is excavated, the vertical stress will be transferred to both sides, and the compressive stress concentration will occur in the surrounding rock on the side wall of the drift. When multiple drifts are excavated, the compressive stress will be redistributed in the formed pillars, and the farther away from the middle drift, the smaller the increased stress. When more than 5 drifts are excavated, the redistributed vertical stress in the ore pillar exceeds the acceptable limit, the chain failure occurs in a short period of time, and the bearing capacity is lost.

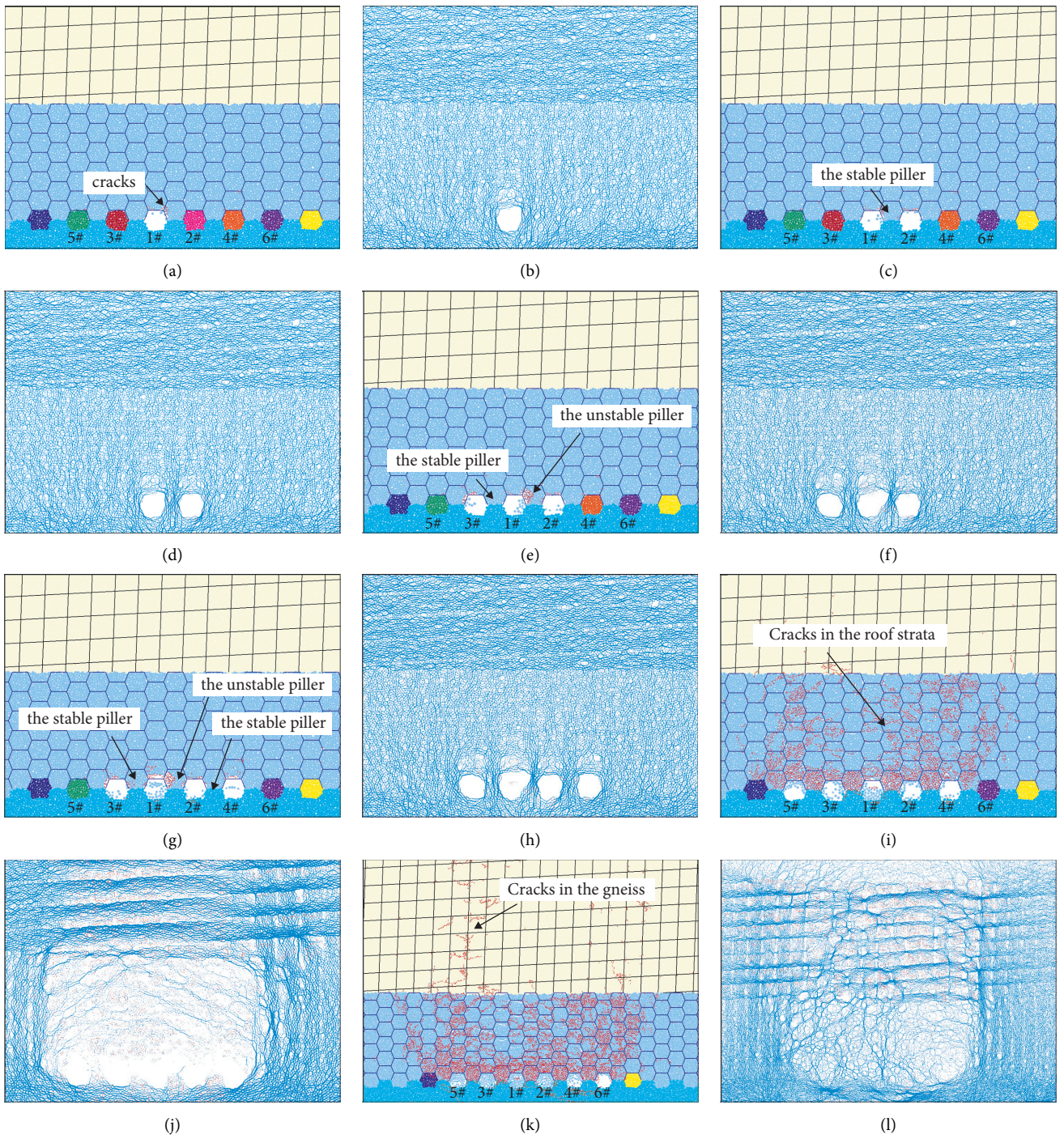

Figure 16: Illustrations of instability process of the pillars and roof. Left: The failure and fracture development of the model. Right: The contact force chain of the model (blue represents pressure and red represents tension). (a)–(b) The 1 # drift is excavated; (c)–(d) The 2 # drift is excavated; (e)–(f) The 3 # drift is excavated; (g)–(h) The 4 # drift is excavated; (i)–(j) The 5 # drift is excavated; (k)–(l) The 6# drift is excavated.

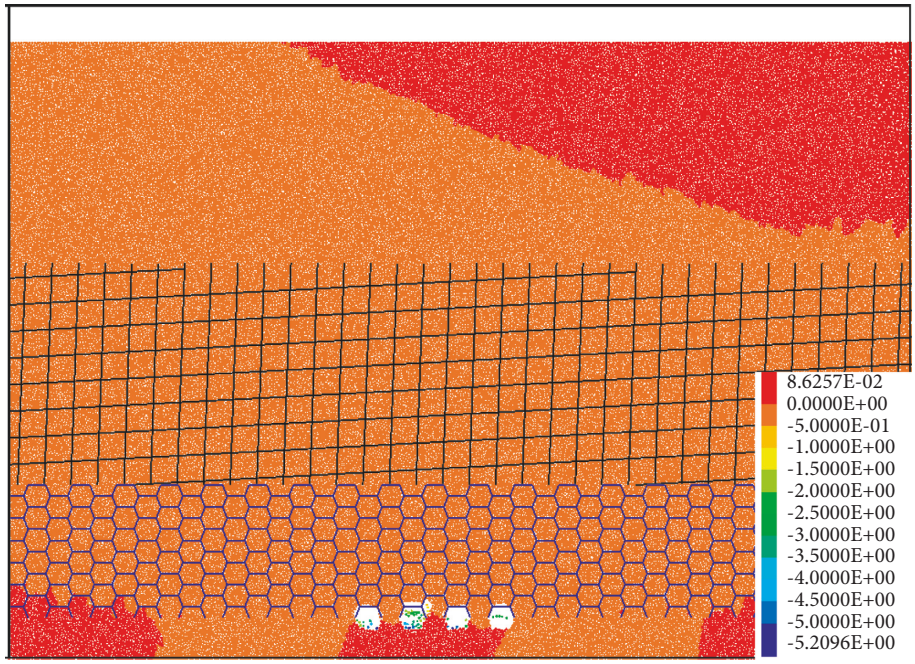

(a)

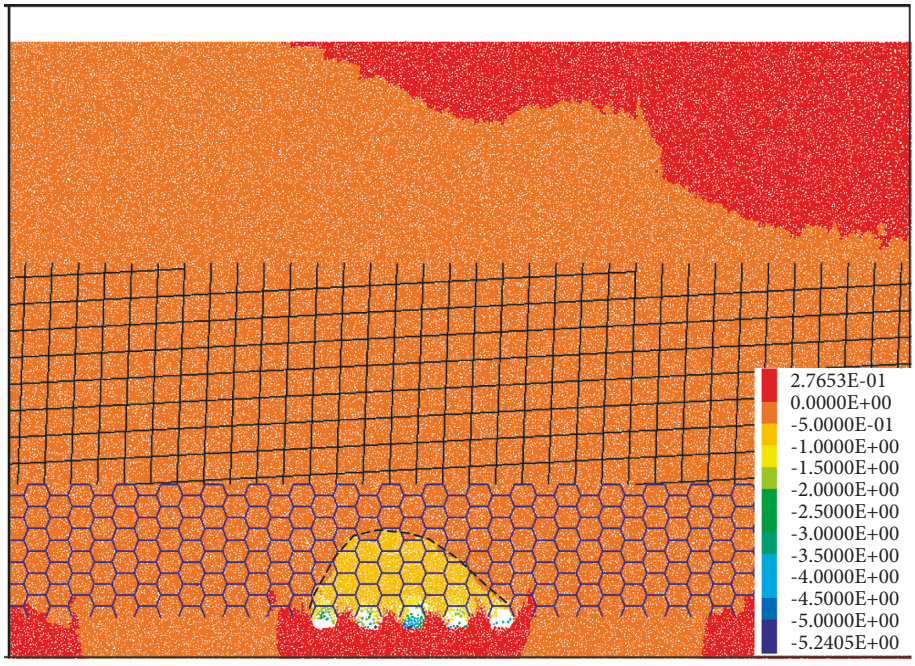

(b)

Figure 17: Continued.

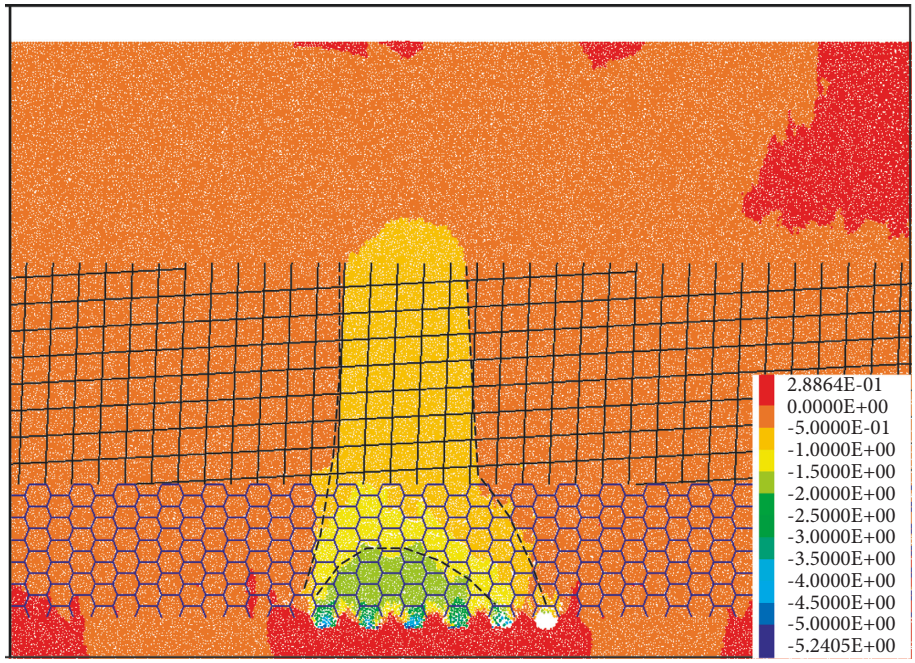

(c)

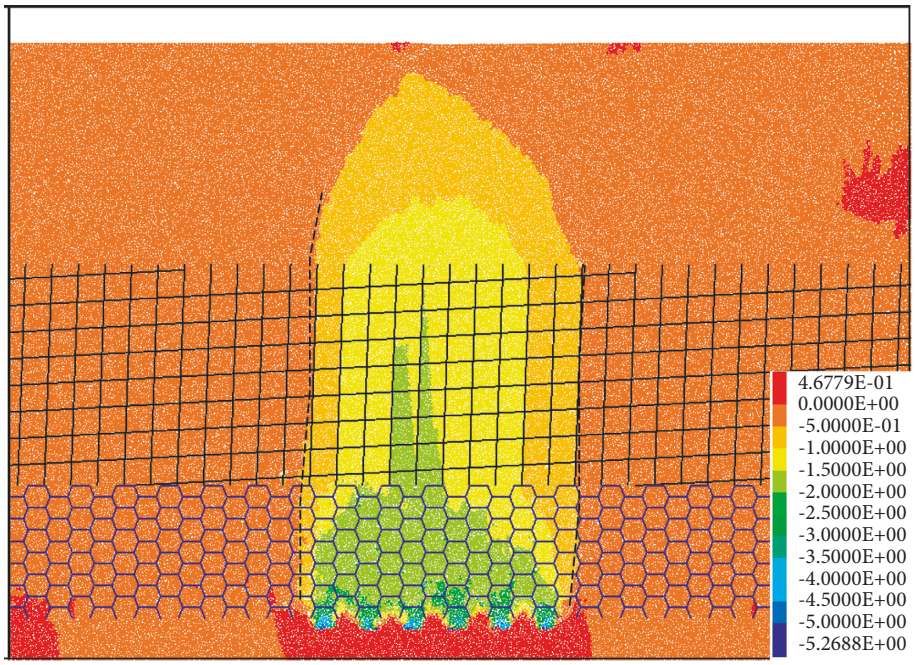

(d)

Figure 17: Displacement cloud diagram of the model during mining process. (a) Steady state of the roof. (b) Arch caving of roof filling body. (c) Initial stage of plug subsidence of overlying gneiss. (d) Late stage of plug subsidence of overlying gneiss.

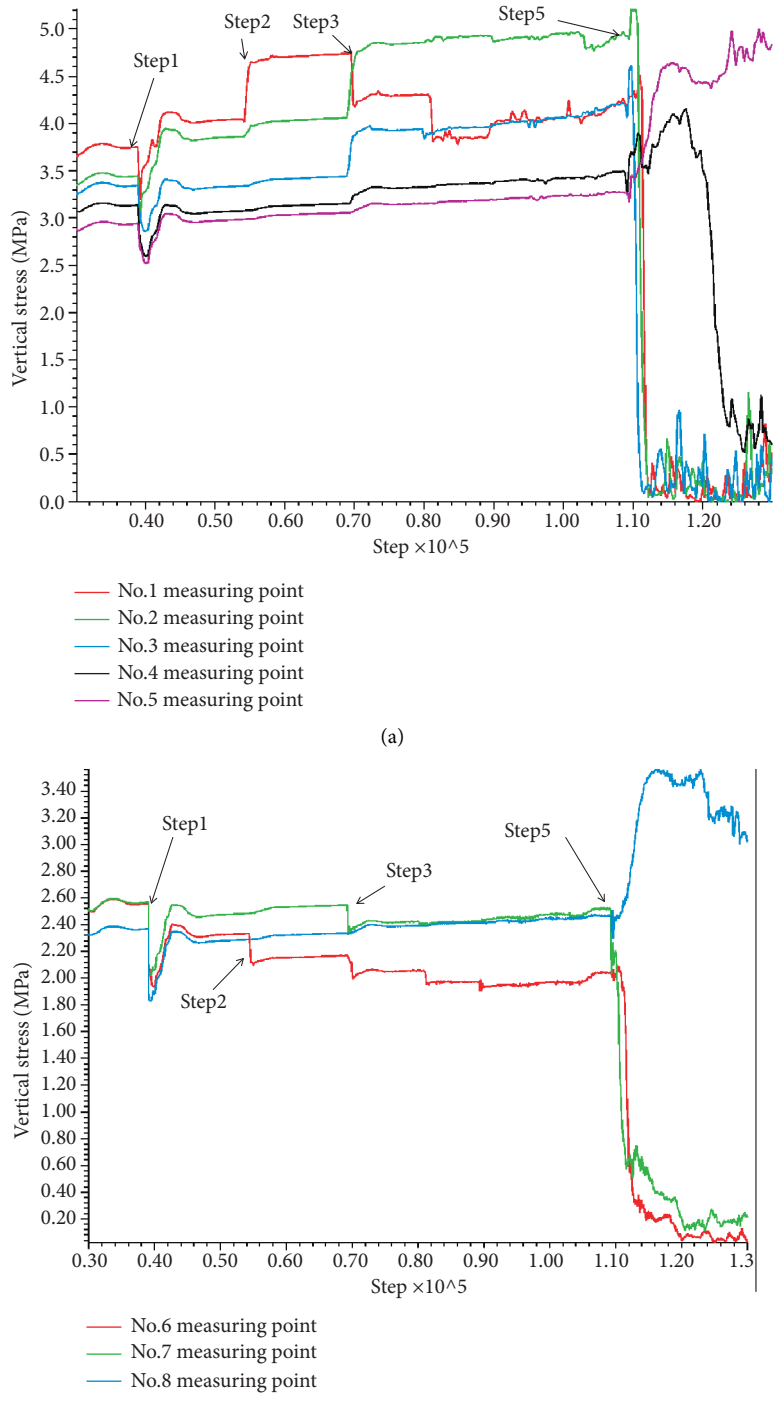

Figure 18: Vertical stress of rock mass during mining. (a) Vertical stress of the pillar during mining. (b) Vertical stress of roof filling body during mining.

It can be seen that the numerical simulation results are very consistent with the field, indicating that the established numerical model can be used to study the mechanism of overburden stratum damage and surface subsidence caused by underground mining in this mine.

6. Conclusions

Field investigation, engineering geological analysis, and the PFC numerical simulation were carried out on the surface collapse accident of a nonferrous mine in northern China using the cemented filling mining method. The mechanism of violent failure of overlying composite strata caused by multiple adjacent narrow goaf was researched. The following conclusions are drawn:

(1) From the field investigation results, it can be seen that the starting position of the underground failure is at the 1613 m level, where the pillar is unstable and damaged, and the roof backfill body is broken and caved. The caving damage caused by the backfill body does not develop to the surface but is terminated below the 1630 m level. Above the 1630 m level, the overall plug subsidence occurred in the rock mass.

(2) The failure process of the overlying rock mass can be divided into four stages due to the special geological conditions of the mine: pillar stability stage, pillar chain failure stage, roof filling caving stage, and gneiss plug settlement stage. According to the method of interval mining, when no more than 4 drifts are mined, the stope can be in a stable state. When more than 4 drifts are mined and cannot be filled in time, the pillars are damaged successively in a short interval. After the chain failure of pillars, the filling material of the roof collapses, and the caving arch develops upward. As the collapsed gravels fill the narrow mine-out areas, the caving failure of the filling body develops to the level of 1625 m and stops. Horizontal joints (dip 3°) make gneiss present a horizontal layered structure, while horizontal in-situ stress is greater than vertical in-situ stress. After the lower filling body loses its bearing capacity, the compression of horizontal in-situ stress keeps the layered gneiss stable for a short time. Under the mining disturbance, this stability is quickly destroyed, and the gneiss above the stope produces overall shear slip along the vertical joints (dip 88°), which eventually leads to the plug subsidence of gneiss.

(3) According to the field investigation, engineering geological analysis and numerical simulation, the roof instability of the narrow goaf deeply buried underground in the mine finally leads to the failure accident of large-scale instantaneous settlement of the surface, which is determined by many factors. Among them, the unique geological condition is the internal cause, and the underground mining activities are the inducement. In the process of surface collapse, the combination of internal and external factors leads to the mechanism of rock stratum movement and the phenomenon of surface damage. Therefore, in order to prevent such damage accident, during mining, the number of continuous mining drifts in any mining area is suggested not to exceed 4, and the next group of drifts should not be exploited before filling the last group.

Data Availability

The data used to support the findings of this study are available and can be demanded from the corresponding author.

Conflicts of Interest

The authors declare that they have no conflicts of interest.

Acknowledgments

The authors would like to thank the financial support provided by the National Natural Science Foundation of China (Grant no. 51534003).

References

[1] X. Cui, Y. Gao, and D. Yuan, "Sudden surface collapse disasters caused by shallow partial mining in Datong coalfield, China," *Natural Hazards*, vol. 74, no. 2, pp. 911–929, 2014.

[2] M. Eremin, E. Gabriel, and I. Smolin, "Numerical simulation of roof cavings in several Kuzbass mines using finite-difference continuum damage mechanics approach," *International Journal of Mining Science and Technology*, vol. 30, no. 2, pp. 157–166, 2020.

[3] S. Wang, X. Li, and S. Wang, "Separation and fracturing in overlying strata disturbed by longwall mining in a mineral deposit seam," *Engineering Geology*, vol. 226, no. 30, pp. 257–266, 2017.

[4] F. G. Bell, T. R. Stacey, and D. D. Genske, "Mining subsidence and its effect on the environment: some differing examples," *Environmental Geology*, vol. 40, no. 1-2, pp. 135–152, 2000.

[5] M. Svartsjaern, "A prognosis methodology for underground infrastructure damage in sublevel cave mining," *Rock Mechanics and Rock Engineering*, vol. 52, no. 1, pp. 247–263, 2019.

[6] E. Can, Ş. Kuşcu, and M. E. Kartal, "Effects of mining subsidence on masonry buildings in Zonguldak hard coal region in Turkey," *Environmental Earth Sciences*, vol. 66, no. 8, pp. 2503–2518, 2012.

[7] L. C. Li, C. A. Tang, X. D. Zhao, and M. Cai, "Block caving-induced strata movement and associated surface subsidence: a numerical study based on a demonstration model," *Bulletin of Engineering Geology and the Environment*, vol. 73, no. 4, pp. 1165–1182, 2014.

[8] A. Vyazmensky, D. Elmo, and D. Stead, "Role of rock mass fabric and faulting in the development of block caving induced surface subsidence," *Rock Mechanics and Rock Engineering*, vol. 43, no. 5, pp. 533–556, 2010.

[9] E. T. Brown, *Block Caving Geomechanics (International Caving Study I, 1997–2000)*, University of Queensland, JKMRC monograph series in mining and mineral processing, Brisbane, 2003.

[10] B. H. G. Brady and E. T. Brown, *Rock Mechanics: For Underground Mining*, Springer, Berlin, 2013.

[11] K. Skrzypkowski, "3D numerical modelling of the application of cemented paste backfill on displacements around strip excavations," *Energies*, vol. 14, no. 22, p. 7750, 2021.

[12] K. Skrzypkowski, "Compressibility of materials and backfilling mixtures with addition of solid wastes from flue-gas treatment and fly ashes," *E3S Web Conf*, vol. 71, p. 7, 2018.

[13] H. Ding, S. Chen, S. Chang, G. Li, and L. Zhou, "Prediction of surface subsidence extension due to underground caving: a case study of hemushan Iron mine in China," *Mathematical Problems in Engineering*, vol. 2020, Article ID 5086049, 10 pages, 2020.

[14] B. Ghabraie, G. Ren, X. Zhang, and J. Smith, "Physical modelling of subsidence from sequential extraction of partially overlapping longwall panels and study of substrata movement characteristics," *International Journal of Coal Geology*, vol. 140, pp. 71–83, 2015.

[15] W. Ren, C. Guo, Z. Peng, and Y. Wang, "Model experimental research on deformation and subsidence characteristics of ground and wall rock due to mining under thick overlying terrane," *International Journal of Rock Mechanics and Mining Sciences*, vol. 47, no. 4, pp. 614–624, 2010.

[16] T. Villegas, E. Nordlund, and C. Dahnér-Lindqvist, "Hangingwall surface subsidence at the Kiirunavaara mine, Sweden," *Engineering Geology*, vol. 121, no. 1-2, pp. 18–27, 2011.

[17] H. Zhao, F. Ma, Y. Zhang, and J. Guo, "Monitoring and mechanisms of ground deformation and ground fissures induced by cut-and-fill mining in the Jinchuan mine 2, China," *Environmental Earth Sciences*, vol. 68, no. 7, pp. 1903–1911, 2013.

[18] X. Song, C. Chen, K. Xia, K. Yang, S. Chen, and X. Liu, "Analysis of the surface deformation characteristics and strata movement mechanism in the main shaft area of Chengchao Iron Mine," *Environmental Earth Sciences*, vol. 77, no. 9, p. 335, 2018.

[19] G. Cheng, T. Ma, C. Tang, H. Liu, and S. Wang, "A zoning model for coal mining - induced strata movement based on microseismic monitoring," *International Journal of Rock Mechanics and Mining Sciences*, vol. 94, pp. 123–138, 2017.

[20] K. Xia, C. Chen, and Y. Deng, "In situ monitoring and analysis of the mining-induced deep ground movement in a metal mine," *International Journal of Rock Mechanics and Mining Sciences*, vol. 109, pp. 32–51, 2018.

[21] N. Xu, P. H. S. W. Kulatilake, H. Tian, X. Wu, Y. Nan, and T. Wei, "Surface subsidence prediction for the WUTONG mine using a 3-D finite difference method," *Computers and Geotechnics*, vol. 48, no. 3, pp. 134–145, 2013.

[22] F. Zhang, T. Yang, L. Li, Z. Wang, and P. Xiao, "Cooperative monitoring and numerical investigation on the stability of the south slope of the Fushun west open-pit mine," *Bulletin of Engineering Geology and the Environment*, vol. 78, no. 4, pp. 2409–2429, 2019.

[23] Q. Wu and P. H. S. W. Kulatilake, "Application of equivalent continuum and discontinuum stress analyses in three-dimensions to investigate stability of a rock tunnel in a dam site in China," *Computers and Geotechnics*, vol. 46, pp. 48–68, 2012.

[24] M. Svartsjaern, D. Saiang, E. Nordlund, and A. Eitzenberger, "Conceptual numerical modeling of large-scale footwall behavior at the Kiirunavaara mine, and implications for deformation monitoring," *Rock Mechanics and Rock Engineering*, vol. 49, no. 3, pp. 943–960, 2016.

[25] S. F. Wang and X. B. Li, "Dynamic distribution of longwall mining-induced voids in overlying strata of a coalbed," *International Journal of Geomechanics*, vol. 17, no. 6, Article ID 04016124, 2017.

[26] T. Villegas and E. Nordlund, "Numerical simulation of the hangingwall subsidence using PFC2D," in *Proceedings of the 5th International Conference and Exhibition on Mass Mining*, Sweden, June 2008.

[27] T. F. V. Barba and E. Nordlund, "Numerical analyses of the hangingwall failure due to sublevel caving: study case," *International Journal of Mining and Mineral Engineering*, vol. 4, no. 3, pp. 201–223, 2013.

[28] M. Svartsjaern and D. Saiang, "Discrete element modelling of footwall rock mass damage induced by sub-level caving at the Kiirunavaara Mine," *Minerals*, vol. 7, no. 7, p. 109, 2017.

[29] L. Zhao and W. Jin-an, "Accident investigation of mine subsidence with application of particle flow code," *Procedia Engineering*, vol. 26, pp. 1698–1704, 2011.

[30] B. Tan, F. Ren, Y. Ning, R. He, and Q. Zhu, "A new mining scheme for hanging-wall ore-body during the transition from open pit to underground mining: a numerical study," *Advances in Civil Engineering*, vol. 2018, Article ID 1465672, 17 pages, 2018.

[31] A. Vyazmensky, D. Stead, D. Elmo, and A. Moss, "Numerical analysis of block caving-induced fa in large open pit slopes: a finite element/discrete element approach," *Rock Mechanics and Rock Engineering*, vol. 43, no. 1, pp. 21–39, 2010.

[32] D. Stead, E. Eberhardt, and J. S. Coggan, "Developments in the characterization of complex rock slope deformation and failure using numerical modelling techniques," *Engineering Geology*, vol. 83, no. 1–3, pp. 217–235, 2006.

[33] E. Trigueros, M. Cánovas, J. Arzúa, and M. Alcaraz, "Stability of an abandoned siderite mine: a case study in northern Spain," *Open Geosciences*, vol. 13, no. 1, pp. 359–376, 2021.

[34] V. I. I. I. Marinos, P. Marinos, and E. Hoek, "The geological strength index: applications and limitations," *Bulletin of Engineering Geology and the Environment*, vol. 64, no. 1, pp. 55–65, 2005.

[35] E. Hoek, C. Carranza-Torres, and B. Corkum, "Hoek–Brown failure criterion-2002 edition," *Proc NARMS-Tac*, vol. 1, no. 1, pp. 267–273, 2002.

[36] K.-S. Woo, E. Eberhardt, D. Elmo, and D. Stead, "Empirical investigation and characterization of surface subsidence related to block cave mining," *International Journal of Rock Mechanics and Mining Sciences*, vol. 61, pp. 31–42, 2013.

[37] D. O. Potyondy and P. A. Cundall, "A bonded-particle model for rock," *International Journal of Rock Mechanics and Mining Sciences*, vol. 41, no. 8, pp. 1329–1364, 2004.

[38] C. J. Li and X. B. Li, "Influence of wavelength-to-tunnel-diameter ratio on dynamic response of underground tunnels subjected to blasting loads," *International Journal of Rock Mechanics and Mining Sciences*, vol. 112, pp. 323–338, 2018.

[39] X. B. Li, C. J. Li, W. Z. Cao, and M. Tao, "Dynamic stress concentration and energy evolution of deep-buried tunnels under blasting loads," *International Journal of Rock Mechanics and Mining Sciences*, vol. 104, pp. 131–146, 2018.

[40] M. I. Diego, *Bonded Particle Model for Jointed Rock Mass*, KTH Royal Institute of Technology, Stockholm, Sweden, 2010.

[41] X. Li, D. Wang, C. Li, and Z. Liu, "Numerical simulation of surface subsidence and backfill material movement induced by underground mining," *Advances in Civil Engineering*, vol. 2019, Article ID 2724370, 17 pages, 2019.

[42] W. Zhao, R. Huang, and M. Yan, "Study on the deformation and failure modes of rock mass containing concentrated parallel joints with different spacing and number based on

smooth joint model in PFC," *Arabian Journal of Geosciences*, vol. 8, pp. 7887–7897, 2015.

[43] M. H. Mehranpour and P. H. S. W. Kulatilake, "Improvements for the smooth joint contact model of the particle flow code and its applications," *Computers and Geotechnics*, vol. 87, pp. 163–177, 2017.

[44] J. A. Vallejos, K. Suzuki, A. Brzovic, and D. M. Ivars, "Application of Synthetic Rock Mass modeling to veined core-size samples," *International Journal of Rock Mechanics and Mining Sciences*, vol. 81, pp. 47–61, 2016.